An Efficient Self-Assembly of CdS Nanowires–Reduced Graphene Oxide Nanocomposites for Selective Reduction of Nitro Organics under Visible Light Irradiation

ARTICLE *in* THE JOURNAL OF PHYSICAL CHEMISTRY C · APRIL 2013

Impact Factor: 4.77 · DOI: 10.1021/jp400550t

5 AUTHORS, INCLUDING:

Nan Zhang
Fuzhou University
49 PUBLICATIONS **3,105** CITATIONS
SEE PROFILE

Yi-Jun Xu
Fujian
109 PUBLICATIONS **6,081** CITATIONS
SEE PROFILE

THE JOURNAL OF PHYSICAL CHEMISTRY C

Article

pubs.acs.org/JPCC

An Efficient Self-Assembly of CdS Nanowires–Reduced Graphene Oxide Nanocomposites for Selective Reduction of Nitro Organics under Visible Light Irradiation

Siqi Liu,[†,‡] Zhang Chen,[†,‡] Nan Zhang,[†,‡] Zi-Rong Tang,[‡] and Yi-Jun Xu*[,†,‡]

[†] State Key Laboratory Breeding Base of Photocatalysis, College of Chemistry and Chemical Engineering, Fuzhou University, Fuzhou, 350002, People's Republic of China

[‡] College of Chemistry and Chemical Engineering, New Campus, Fuzhou University, Fuzhou, 350108, People's Republic of China

Supporting Information

ABSTRACT: The CdS nanowires–reduced graphene oxide nanocomposites (CdS NWs–RGO NCs) combining one-dimensional (1-D) with two-dimensional (2-D) structures are successfully synthesized by a simple and efficient electrostatic self-assembly method, followed by a hydrothermal reduction process. The probe reactions for photocatalytic selective reduction of aromatic nitro organics in water under visible light irradiation are utilized to evaluate the photoactivity of the as-prepared CdS NWs–RGO NCs. The CdS NWs–RGO NCs exhibit significantly enhanced photoactivity as compared with the CdS nanowires (CdS NWs). The addition of RGO into the matrix of CdS NWs in a controlled manner is able to efficiently enhance the lifetime and transfer of photogenerated charge carriers from CdS NWs under visible light irradiation. Furthermore, the presence of RGO also improves the adsorption capacity of CdS NWs–RGO NCs toward aromatic nitro organics. These two primary factors result in the drastic photoactivity improvement of CdS NWs–RGO NCs toward selective reduction of nitro organics to the corresponding amino organics in water under visible light irradiation. In addition, the possible photocatalytic reaction mechanism is proposed. It is hoped that our work could not only offer useful information on the fabrication of various specific 1-D semiconductor–2-D RGO nanocomposites but also open a new window of such 1-D semiconductor–2-D RGO nanocomposites as visible light photocatalyst in the promising field of selective organic transformations.

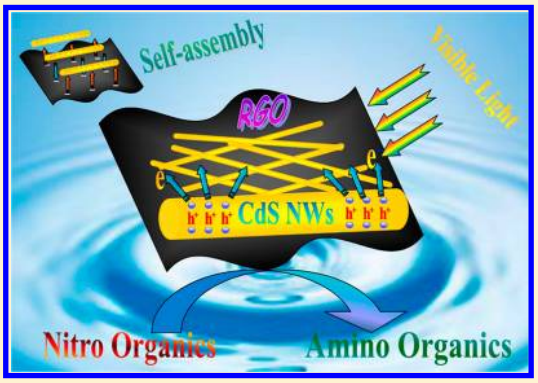

1. INTRODUCTION

Heterogeneous photocatalysis by semiconductor materials has been gaining increasing interest due to its promising potential for solar energy conversion.[1−19] Notably, most studies are mainly focused on efficient photocatalytic nonselective mineralization of toxic organic pollutants to CO_2 and H_2O and water splitting to H_2 or O_2. In contrast, the application of semiconductor-based photocatalysis in "selective" organic transformations is relatively uncommon.[20−23] However, the rational use of appropriate semiconductors and fine control of reaction conditions can promote organic reactions to occur with high selectivity, as has been witnessed by recent progress on photocatalytic selective reduction of nitro organics over various semiconductor-based materials,[24−29] which could be used as an alternative green method for fine chemicals production. For example, Ferry and Glaze have investigated the mechanism of photocatalytic reduction of nitro organics on the surface of Degussa P25 in the absence of oxygen and in the presence of a sacrificial electron donor methanol or isopropanol.[26] They proposed that the photocatalytic reduction of nitro organics proceeds by the sequence process RNO_2–RNO–RNH_2, although the hydroxylamine intermediate is not clearly detected. They also found that the radicals generated from alcohol oxidation are not the active reducing agents.[26] Brezova et al. have confirmed the formation of only one stable radical, $C_6H_5N^{\bullet}OH$, corresponding to the nitrobenzene photoreduction. The production of hydroxyalkyl radicals, such as $^{\bullet}CH(OH)CH_3$ in the case of ethanol being used as an electron donor, is via the reaction with photogenerated TiO_2 valence band holes.[27] Tada et al. demonstrated that, over the photocatalyst of Ag clusters deposited on TiO_2, the direct electron reduction is more advantageous than the indirect reduction by hydroxyalkyl radicals if a higher nitrobenzene concentration is used.[28]

It is commonly accepted that photogenerated electrons play a key role in the photocatalytic selective reduction reaction.[28−30] Thus, improving the utilization efficiency of photogenerated electrons and prolonging the photogenerated charge carriers' lifetime are expected to enhance the photoactivity for selective reduction of nitro organics. In this regard,

Received: January 17, 2013
Revised: March 24, 2013
Published: March 26, 2013

one-dimensional (1-D) semiconductor materials with unique structures and morphologies could be a promising choice,[4,31−51] because 1-D semiconductor materials (e.g., nanowires or nanotubes) with high length-to-diameter ratios are particularly attractive for use in photocatalytic reduction owing to their excellent fast and long-distance electron-transport capability, large surface areas and pore volumes, and enhanced light absorption and scattering.[52−58] On the other hand, recent years have witnessed immense interest in synthesis of graphene (GR)−semiconductor composite photocatalysts, aiming to use the excellent electron conductivity of the 2-D graphene network to prolong the fate of photogenerated electron−hole pairs, which improves the photoactivity toward nonselective degradation of pollutants, water splitting, and selective organic transformation.[13,15,32,59,60] Thus, a proper integration of (1-D) semiconductor materials with 2-D graphene in an appropriate manner would further improve the photoactivity toward target reactions.

Although some 1-D semiconductor nanowires−GR composites have been reported for utilization in solar cells, piezoelectric nanogenerators, and gas sensors,[61−63] the reports on 1-D semiconductor nanowires−GR composites for photocatalytic applications are rather scarce. Especially, forthputting the unique 1-D semiconductor nanowires−GR composites into photocatalytic selective reduction of nitro organics under visible light has remained unavailable so far. As a well-known II−VI semiconductor, CdS features a suitable band gap (2.4 eV) corresponding well with the spectrum of sunlight.[64−68] Therefore, it can be reasonably expected that the CdS nanowires−GR nanocomposites can combine unique 1-D and 2-D structures along with their respective excellent electron conductivity, thereby exhibiting significantly enhanced photoactivity toward selective reduction of nitro organics under visible light irradiation.

Herein, we predominantly focus on the synthesis of CdS nanowires (CdS NWs)−reduced graphene oxide (RGO) nanocomposites (CdS NWs−RGO NCs) and, specifically, their application toward selective reduction of aromatic nitro organics under visible light irradiation. Since graphene oxide (GO) is used as the precursor of graphene (GR), we herein denote GR prepared from reduction of GO as RGO for clarity. The synthesis of CdS NWs−RGO NCs is via a simple self-assembly approach, which is afforded by a substantial electrostatic attractive interaction between positively charged CdS NWs and negatively charged GO in an aqueous solution, followed by a hydrothermal reduction of GO to RGO. The as-synthesized CdS NWs−RGO NCs exhibit remarkably enhanced visible light photoactivity toward selective reduction of nitro organics as compared to the original CdS NWs. The origin accounting for the improved photoactivity and the underlying reaction mechanism have been studied in terms of a series of characterization and controlled experiments using radicals scavengers. To the best of our knowledge, this work represents a first example to use the 1-D semiconductor NWs-RGO NCs photocatalyst for selective organic reduction reaction under ambient conditions. It is hoped that this work could open a new doorway of synthesis of such 1-D semiconductor−RGO composites by such a simple and efficient electrostatic self-assembly strategy and their application as visible light photocatalysts toward selective organic transformations.

2. EXPERIMENTAL SECTION

2.1. Preparation. *Materials.* Sodium diethyldithiocarbamate trihydrate ($C_5H_{10}NNaS_2·3H_2O$), cadmium chloride ($CdCl_2·2.5H_2O$), ethylenediamine ($C_2H_8N_2$), (3-aminopropyl) triethoxysilane ($C_9H_{23}NO_3Si$, APTES), graphite powder, sulfuric acid (H_2SO_4), nitric acid (HNO_3), hydrochloric acid (HCl), potassium persulfate ($K_2S_2O_8$), phosphorus pentoxide (P_2O_5), hydrogen peroxide, 30% (H_2O_2), potassium permanganate ($KMnO_4$), and ethanol (C_2H_6O) were obtained from Sinopharm Chemical Reagent Co., Ltd. (Shanghai, China). All materials were analytical grade and used as received without further purification. Deionized water used in the synthesis was from local sources.

Synthesis. The CdS NWs−RGO nanocomposites (CdS NWs−RGO NCs) have been fabricated by a simple and efficient electrostatic self-assembly method, followed by a hydrothermal reduction with ethanol and deionized water, as illustrated in Scheme 1. (I) Fabrication of CdS nanowires:

Scheme 1. Schematic Flowchart for Synthesis of CdS NWs−RGO NCs by an Electrostatic Self-Assembly Method, Followed by a Hydrothermal Reduction Process

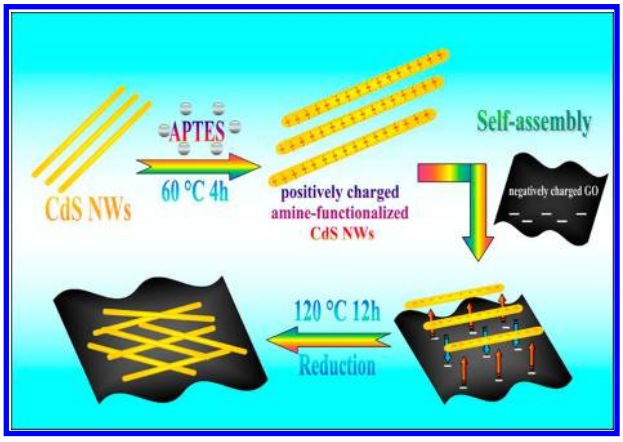

Uniform CdS NWs were grown through a modified method.[52,69] The detail of the typical process is presented in the Supporting Information. (II) Synthesis of graphene oxide (GO): GO was synthesized from natural graphite powder by a modified Hummers method.[13,32,60,70−73] The detail of the typical process is presented in the Supporting Information. (III) Synthesis of CdS NWs−RGO NCs by electrostatic self-assembly of CdS NWs on the framework of RGO: A 0.4 g portion of CdS NWs was first dispersed in 200 mL of ethanol by sonication for 30 min. APTES (2 mL) was then added, heated, and refluxed for 4 h. APTES-treated CdS NWs were sufficiently rinsed with ethanol to wash away any remaining APTES moiety. A negatively charged GO suspension in water (0.2 mg·mL^{-1})[74] was added into the positively charged amine-functionalized[74] CdS NWs dispersion in water with the weight ratio of GO to CdS NWs at 0.05:1 under vigorous stirring at pH = 6. After mixing for 30 min, the mixture was centrifuged and washed with deionized water. For the reduction of GO to RGO, a hydrothermal process was used as follows. CdS NWs−GO NCs (0.4 g) were dispersed in a solution of ethanol (20 mL) and deionized water (60 mL), then autoclaved in a Teflon-lined stainless steel vessel at 120 °C for 12 h. The dark green precipitates thus obtained were collected, washed thoroughly with deionized water, and then dried in an oven at 60 °C.

dx.doi.org/10.1021/jp400550t | J. Phys. Chem. C 2013, 117, 8251−8261

2.2. Characterization. Zeta potential (ξ) measurements of the samples were determined by dynamic light-scattering analysis (Zeta sizer 3000HSA) at a room temperature of 25 °C. In brief, 25 mg of the sample was dispersed in 50 mL of deionized water to obtain a concentration of ca. 500 mg·L^{-1} in an aqueous solution. The pH adjustment was achieved by diluted 0.1 M HCl or NaOH aqueous solution when the zeta potential of the sample was measured as a function of pH value. The crystal phase properties of the samples were analyzed with a Bruker D8 Advance X-ray diffractometer (XRD) using Ni-filtered Cu Kα radiation at 40 kV and 40 mA in the 2θ range from 5° to 80° with a scan rate of 0.02° per second. The optical properties of the samples were characterized by a Cary 500 UV−visible ultraviolet/visible diffuse reflectance spectrophotometer (DRS), during which $BaSO_4$ was employed as the internal reflectance standard. Field-emission scanning electron microscopy (FE-SEM) was used to determine the morphology of the samples on an FEI Nova NANOSEM 230 spectrophotometer. Transmission electron microscopy (TEM) images were obtained using a JEOL model JEM 2010 EX instrument at an accelerating voltage of 200 kV. X-ray photoelectron spectroscopy (XPS) measurements were performed using a Thermo Scientific ESCA Lab250 spectrometer, which consists of monochromatic Al Kα as the X-ray source, a hemispherical analyzer, and sample stage with multiaxial adjustability to obtain the composition on the surface of samples. The Fourier transformed infrared spectroscopy (FT-IR) was performed on a Nicolet Nexus 670 FT-IR spectrophotometer at a resolution of 4 cm^{-1}. The Brunauer−Emmett−Teller (BET) specific surface area (S_{BET}) of the samples was analyzed by nitrogen (N_2) adsorption−desorption in a Micromeritics ASAP 2020 apparatus. The photoluminescence (PL) spectra for solid samples were investigated on an Edinburgh FL/FS900 spectrophotometer with an excitation wavelength of 365 nm. Photoelectrochemical measurements were performed in a homemade three-electrode quartz cell with a PAR VMP3Multi Potentiotat apparatus. A Pt plate was used as counter electrode, and Ag/AgCl electrodes were used as reference electrodes, while the working electrode was prepared on fluoride tin oxide (FTO) conductor glass. The sample powder (6 mg) was ultrasonicated in 0.5 mL of *N*,*N*-dimethylflormamide (DMF, supplied by Sinopharm Chemical Reagent Co., Ltd.) to disperse it evenly to get a slurry. The slurry was spread onto FTO glass, whose side part was previously protected using Scotch tape. The working electrode was dried overnight under ambient conditions. A copper wire was connected to the side part of the working electrode using conductive tape. Uncoated parts of the electrode were isolated with epoxy resin. The electrolyte was 0.2 M aqueous Na_2SO_4 solution (pH = 6.8) without additive. The visible light irradiation source was a 300 W Xe arc lamp system equipped with a UV−CUT filter (λ > 420 nm).

2.3. Photocatalytic Activity. In a typical photocatalytic reaction, a 300 W Xe arc lamp (PLS-SXE 300, Beijing Perfect Light Co., Ltd.) with a UV−CUT filter to cut off light with a wavelength λ < 420 nm was used as the irradiation source. A 10 mg portion of the sample was added into 30 mL of the aromatic nitro compounds solution (20 mg·L^{-1}) in a quartz vial. Before visible light illumination, the above suspension was stirred in the dark for 1 h to ensure the establishment of an adsorption−desorption equilibrium between the sample and reactant. During the process of the reaction, 3 mL of sample solution was collected at a certain time interval and centrifuged to remove the catalyst completely at 12 000 rmp. Afterward, the solution was analyzed on a Varian ultraviolet−visible light (UV−vis) spectrophotometer (Cary-50, Varian Co.). The whole experimental process was conducted under N_2 bubbling at the flow rate of 80 mL·min^{-1}. The photograph of the experimental setup is displayed in the Supporting Information (Figure S1).

3. RESULTS AND DISCUSSION

The electrostatic self-assembly process of CdS NWs with GO can be demonstrated by the zeta potential (ξ) measurements. Figure S2 (in the Supporting Information) shows ξ values of amine (APTES)-functionalized CdS NWs and GO as a function of pH. It is seen in Figure S2A (in the Supporting Information) that the amine-functionalized CdS NWs show a zeta potential value of +40.6 mV when dispersed in water without adding HCl or NaOH aqueous solution at pH = 6. That indicates a positively charged surface of amine-functionalized CdS NWs dispersion in water at pH = 6. Considering the fact of the decomposition of CdS in the strong acid and alkali environment, the zeta potential analysis at different pH values is not tested. The zeta potential analysis on the GO colloidal dispersion in water, as shown in Figure S2B (in the Supporting Information), reveals a significantly negatively charged surface with excellent stabilization in the whole pH regime (2−12). The negatively charged surface of GO colloids is ascribed to the deprotonation of the carboxyl groups (−COOH) during the dialysis process in the synthesis of GO.[75,76] The stabilization of GO colloids in this wide pH range is due to electrostatic repulsions between negatively charged GO. Thus, it is clear that, with the control of pH = 6 in an aqueous solution, the positively charged amine-functionalized CdS NWs and negatively charged GO can spontaneously establish a solid basis of electrostatic attraction for the self-assembly construction of the nanocomposites of CdS NWs−GO. This is followed by the hydrothermal reduction of GO to RGO, thereby the CdS NWs−RGO NCs are obtained, as pictorially illustrated in Scheme 1. In addition, a zeta potential titration experiment has also been performed to support the electrostatic self-assembly process. As shown in Figure S3 (in the Supporting Information), with adding increasing amounts of positively charged CdS NWs into the negatively charged GO, the zeta potential values are gradually changed from negative to positive, which indicates the occurrence of the electrostatic attraction.

Scanning electron microscopy (SEM) images and transmission electron microscopy (TEM) images are taken to directly analyze the microscopic morphology and structure information of the CdS NWs and CdS NWs-RGO NCs. It is shown in Figure 1A that the as-prepared CdS NWs exhibit the characteristic 1-D morphology with an average diameter of ca. 50−100 nm. The dimensions are highly uniform among the individual CdS NWs. After the electrostatic attraction between CdS NWs and GO, followed by hydrothermal reduction of GO to RGO, it can be seen from Figure 1B that the RGO sheet and semiconductor CdS NWs ingredients have been integrated by the way of an intimate interfacial contact. It is reasonable for this intimate interfacial contact, considering that, during the electrostatic self-assembly process, the electrostatic attractive interaction between positively charged amine-functionalized CdS NWs and negatively charged GO makes the two ingredients undergo a relatively adequate interfacial interaction. As can be seen from the TEM analysis in Figure 2A,B, curly

dx.doi.org/10.1021/jp400550t | J. Phys. Chem. C 2013, 117, 8251−8261

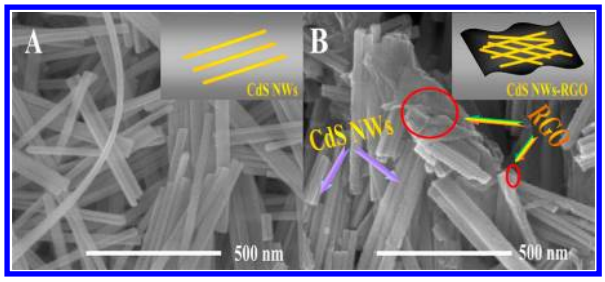

Figure 1. Typical SEM images of the as-prepared samples of CdS NWs (A) and CdS NWs–RGO NCs (B); the insets of (A) and (B) are the corresponding schematic model.

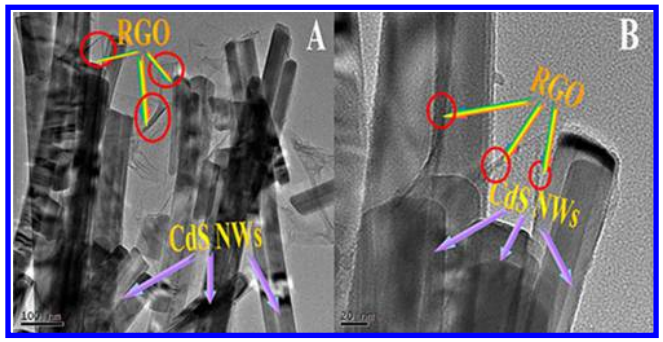

Figure 2. Typical TEM images of the as-prepared samples of CdS NWs–RGO NCs at different magnifications.

RGO sheets have an adequate interfacial contact with CdS NWs, and it is also clear to see that some CdS NWs are even wrapped by the RGO sheets, which is in agreement with the SEM results. The joint SEM and TEM characterization suggests a good interfacial contact formed between the 1-D CdS NWs and the 2-D RGO sheets. Because the transfer process of charge carriers in RGO–semiconductor nanocomposites is intimately related with the interfacial interaction between RGO and the semiconductor,[32,60,77] it could be expected that such a good interfacial contact for the CdS NWs–RGO NCs should favor the charge carrier transfer process.

Figure 3 shows the X-ray diffractometer (XRD) patterns of the samples CdS NWs and CdS NWs–RGO NCs. The XRD pattern of CdS NWs can be ascribed to the stable hexagonal phase CdS (JCPDS No. 41-1049). The peaks at 2θ values of

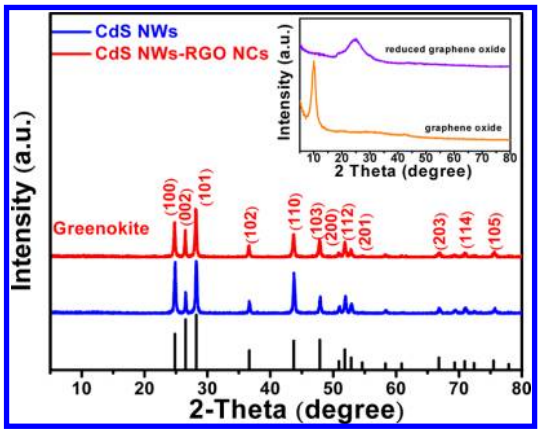

Figure 3. XRD patterns of the as-prepared CdS NWs and CdS NWs–RGO NCs; the inset is the XRD patterns of the graphene oxide (GO) and reduced graphene oxide (RGO).

24.8, 26.5, 28.2, 36.6, 43.7, 47.9, 50.9, 51.8, 52.8, 66.8, 69.2, 70.9, 72.3, and 75.4° for CdS NWs are indexed to the (100), (002), (101), (102), (110), (103), (200), (112), (201), (203), (210), (211), (114), and (105) crystal planes of greenokite structure CdS with a hexagonal phase, respectively. The CdS NWs–RGO NCs exhibit the similar diffraction peaks to that of CdS NWs. However, no typical diffraction peaks of RGO are observed in the CdS NWs–RGO NCs. This is because the main characteristic peak of RGO at 25.0° is very weak, which may be overlapped with the strong (100) peak of greenokite CdS. In addition, no typical diffraction peaks of GO at ca.10.8° and 43.0° can also be observed, indicating the successful reduction of GO to RGO through the hydrothermal process.[60,78–81]

The efficient reduction of GO to RGO after the hydrothermal treatment can also be evidenced by the contrast comparison of the C 1s X-ray photoelectron spectra (XPS) of GO and CdS NWs–RGO NCs, which is displayed in Figure S4A,B (in the Supporting Information). For the bare GO, the C 1s XPS spectra suggest the abundance of various oxygen-containing functional groups on the GO surface. For the CdS NWs–RGO NCs, the significant loss of oxygen-containing functional groups is observed based on the C 1s XPS spectra in Figure S4B (in the Supporting Information), which indicates the sufficient reduction of GO to RGO after the hydrothermal reduction treatment.[32,60,82] The XPS result is in good agreement with the Fourier transformed infrared spectroscopy (FT-IR), as shown in Figure S5 (in the Supporting Information). According to the FT-IR data, the apparent loss of peaks corresponding to various oxygen-containing functional groups indicates the reduction of GO to RGO after the hydrothermal treatment process.

The ultraviolet–visible light (UV–vis) diffuse reflectance spectra (DRS) are used to determine the optical properties of the samples. It can be seen from Figure 4A that, as compared to the sample CdS NWs, the introduction of RGO has a significant effect on the optical property of the visible light absorption region ranging from 500 to 800 nm for the sample CdS NWs–RGO NCs, which is in accordance with the color change of the samples from yellow to dark green, as shown in Figure S6 (in the Supporting Information). The enhanced absorption capability of visible light of CdS NWs–RGO NCs suggests that it might have the higher photocatalytic activity for target reactions under visible light irradiation. A plot obtained via the transformation based on the Kubelka–Munk function versus the energy of light is shown in Figure 4B. The estimated band-gap values of the samples are about 2.4 and 2.3 eV, approximately, corresponding to CdS NWs and CdS NWs–RGO NCs, respectively. This indicates a band-gap narrowing of the CdS NWs due to the introduction of RGO into the matrix of CdS NWs. Such an analogous phenomenon is also observed in previous research studies regarding semiconductor–RGO nanocomposites, which can be attributed to the interfacial interaction between the semiconductor and the RGO support.[13,32,60,8]

The photocatalytic activity of CdS NWs–RGO NCs has been evaluated by selective reduction of nitro organics to corresponding amino organics in the aqueous phase under visible light irradiation with the addition of ammonium formate as a quencher for photogenerated holes and N_2 purge under ambient conditions, that is, room temperature and atmospheric pressure. Figure 5 shows the contrast photocatalytic performance between CdS NWs and CdS NWs–RGO NCs for

dx.doi.org/10.1021/jp400550t | J. Phys. Chem. C 2013, 117, 8251–8261

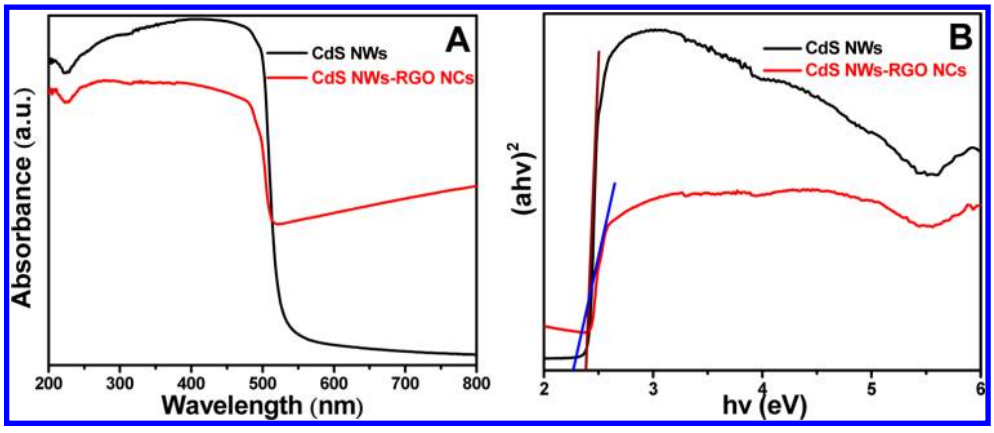

Figure 4. UV−vis diffuse reflectance spectra (DRS) of the samples of CdS NWs and CdS NWs−RGO NCs (A) and the plot of transformed Kubelka−Munk function versus the energy of light (B).

selective reduction of nitro organics. In the light of photoactivity data, it is clear to see that the CdS NWs−RGO NCs exhibit a remarkably enhanced photoactivity as compared to CdS NWs toward selective reduction of nitro organics to the corresponding amino organics under visible light irradiation. Taking the photocatalytic selective reduction of 4-nitroaniline (4-NA) to 4-phenylenediamine (4-PDA) as an example, shown in Figure 5A, we can see that, over the CdS NWs−RGO NCs, 4-NA can almost be reduced completely with 10 min of visible light irradiation, which shows a much higher photoactivity than that for CdS NWs. The conversion of the 4-NA to 4-PDA is monitored by the ultraviolet−visible light adsorption spectra (Figure S7, in the Supporting Information), which indicates that there are only two principal species, 4-NA and 4-PDA, during the reduction process with reaction time. This is further corroborated by the high-performance liquid chromatograph (HPLC) spectra, as shown in Figure S8 (in the Supporting Information). However, due to the purity of the reagents, it is inevitable to observe some minor impurity peaks. In addition, a very minor peak is also observed in the HPLC spectra, which could be ascribed to intermediate products.[26] However, it is clear to see that the impurity and intermediate peaks are very weak, which thus suggests that the very high selectivity is achieved for photocatalytic reduction of nitro organics to amino organics. Such a similar photoactivity enhancement trend has also been observed in the case of selective reduction of other aromatic nitro compounds, such as 2-nitroaniline, 4-nitrophenol, 1-bromo-4-nitrobenzene, 4-nitroanisole, and 4-nitrotoluene, as displayed in Figure 5B−F.

To understand the origin accounting for the drastic enhanced photoactivity of CdS NWs−RGO NCs for selective reduction of nitro organics as compared to CdS NWs, we have further characterized these two samples using the photoelectrochemical analysis and photoluminescence (PL) spectra, which are able to reflect the fate and transfer of photogenerated charge carriers that, in principle, are the key factors determining the overall photoactivity associated with semiconductor-based materials.[50,51,60,68,77,83] As mirrored in Figure 6A, transient photocurrent responses of CdS NWs and CdS NWs−RGO NCs over several on−off cycles of intermittent visible light irradiation (λ > 420 nm) are observed with good reproducibility. It is well-known that photocurrent originates from the diffusion of the photogenerated electrons to the back contact, and meanwhile, the photoinduced holes are taken by the hole acceptor in the electrolyte.[84] The much higher photocurrent responses of CdS NWs−RGO NCs than CdS NWs suggest the more efficient separation and longer lifetime of photoexcited electron−hole pairs of CdS NWs−RGO NCs than those of CdS NWs. The sharp attenuation of the photocurrent is observed with the light off, indicating the recombination of photoexcited electrons and holes. On the other hand, Figure 6B shows the result of electrochemical impedance spectroscopy (EIS), which reflects the fact that the impedance arc radius of the CdS NWs−RGO NCs is smaller than that of CdS NWs, indicating that CdS NWs−RGO NCs demonstrate enhanced conductive capability as compared with CdS NWs. These results are understandable because RGO has an excellent capability of capturing, storing, and shuttling electrons through its sp^2 network.[13,32,68,77,83,85−87] Thus, the presence of RGO in CdS NWs−RGO NCs is able to lead to decreasing the likelihood of the recombination of photoexcited electron−hole pairs from semiconductor CdS NWs, which thus results in a prolonged lifetime of charge carriers. This is in accordance with the higher photocatalytic activity of CdS NWs−RGO than CdS NWs, as observed above. The more efficient separation and longer lifetime of photoexcited electron−hole pairs of CdS NWs−RGO NCs than CdS NWs have also been confirmed by the photoluminescence (PL) spectra. On the basis of PL data, as displayed in Figure 7, under an excitation wavelength of 365 nm, the PL intensity obtained over CdS NWs−RGO NCs is much weaker than that of CdS NWs, thus suggesting the longer lifetime of photogenerated charge carriers from CdS NWs−RGO NCs. The two distinct emission bands at about 540 and 620 nm can be observed, which is consistent with the previous reports.[88−92] The former one can be assigned to near-band-edge emission, and the latter is associated with structural defects that may arise from the excess of sulfur or core defects on the nanowire surfaces.[88−92] These charge carriers with prolonged lifetime photoinduced from CdS NWs−RGO NCs are beneficial for the enhanced photocatalytic activity over the original CdS NWs. In addition, it should be noted that, in our reaction system, the photogenerated positive holes are quenched by the addition of ammonium formate, thus offering an adequate opportunity of contact between photogenerated electrons and reactants (nitro organics), which results in the increased photocatalytic activity of the samples.

To prove that the selective reduction of nitro organics is driven by photogenerated electrons, we have further performed controlled experiments with the addition of an electron scavenger, $AgNO_3$.[22] Figure 8 shows the photocatalytic

dx.doi.org/10.1021/jp400550t | J. Phys. Chem. C 2013, 117, 8251−8261

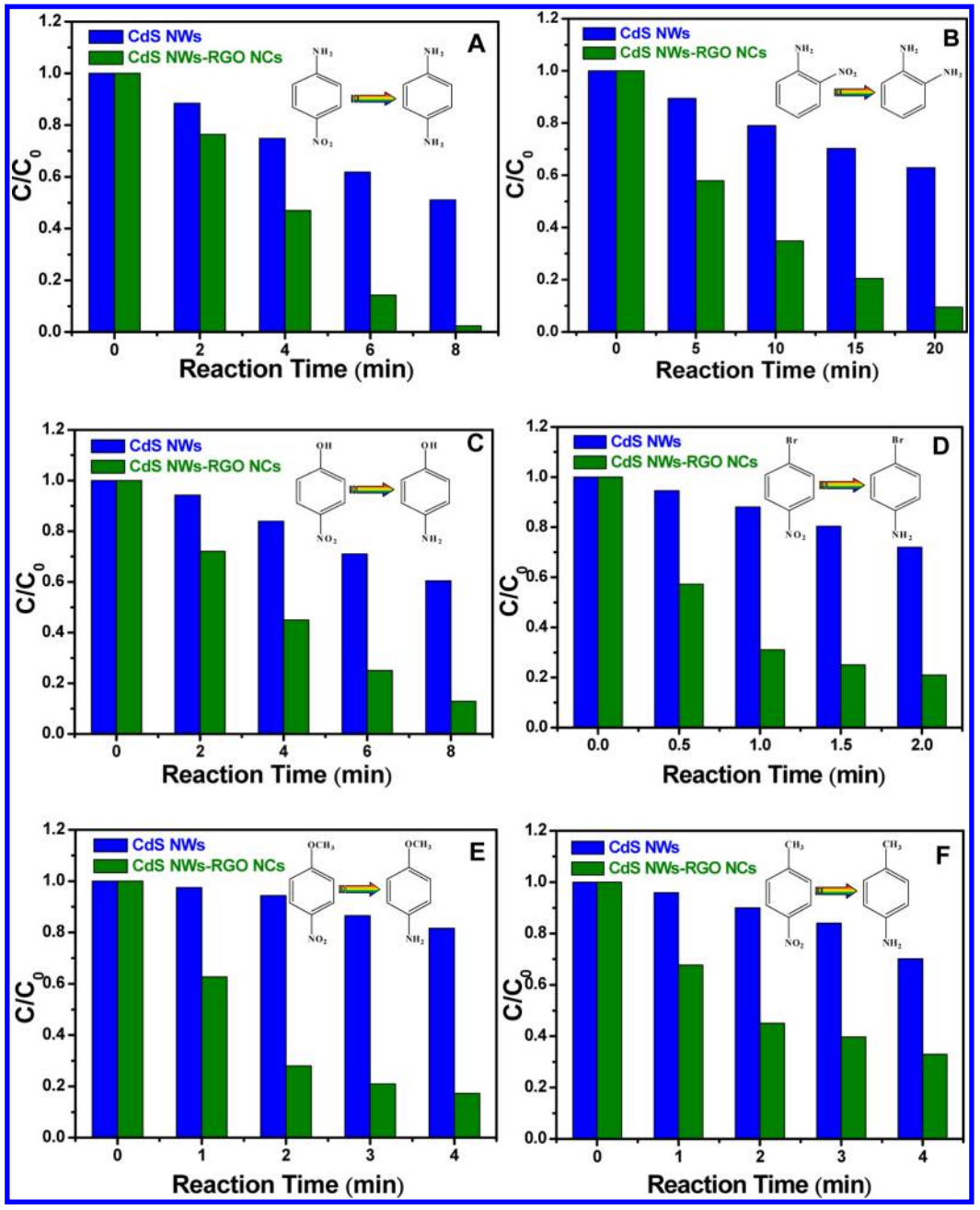

Figure 5. Photocatalytic performance of the as-prepared CdS NWs and CdS NWs−RGO NCs for aromatic nitro compound reduction under visible light irradiation ($\lambda > 420$ nm) with the addition of ammonium formate as a quencher for photogenerated holes and N_2 purge at room temperature in the aqueous phase: (A) 4-nitroaniline; (B) 2-nitroaniline; (C) 4-nitrophenol; (D) 1-bromo-4-nitrobenzene; (E) 4-nitroanisole, and (F) 4-nitrotoluene.

performances of both CdS NWs and CdS NWs−RGO NCs with or without adding the electron scavenger, $AgNO_3$. As displayed in Figure 8A, when 40 mg of $AgNO_3$ is added into the 4-NA reduction system under visible light irradiation ($\lambda >$ 420 nm) in the aqueous phase over CdS NWs, no conversion of 4-NA is observed. Figure 8B shows the same phenomenon of terminating reduction of 4-NA in the aqueous phase over CdS NWs−RGO NCs. These clearly indicate that the reduction reactions of both CdS NWs and CdS NWs−RGO NCs are driven by the photogenerated electrons. The introduction of RGO into the matrix of CdS NWs in CdS NWs−RGO NCs prolongs the lifetime of photogenerated charge carriers and increases the contact efficiency of photogenerated electrons with reactants, thereby causing the significant enhancement of photocatalytic activity, as observed above. In addition, cycling photoreduction experiments are also conducted to investigate the photostability of the samples. Figure 9 displays the data of cycling experiments of reduction of 4-NA over the CdS NWs−RGO NCs photocatalyst under irradiation of visible light ($\lambda >$ 420 nm). The result indicates that no noticeable activity change is observed during four successive recycles, suggesting that the CdS NWs−RGO NCs photocatalyst is stable during the photocatalytic reduction reaction. Additionally, XRD patterns (Figure S9 in the Supporting Information) of the fresh and used samples reveal an intact crystalline structure of the CdS NWs−RGO NCs scaffold after recycled photocatalytic

dx.doi.org/10.1021/jp400550t | J. Phys. Chem. C 2013, 117, 8251−8261

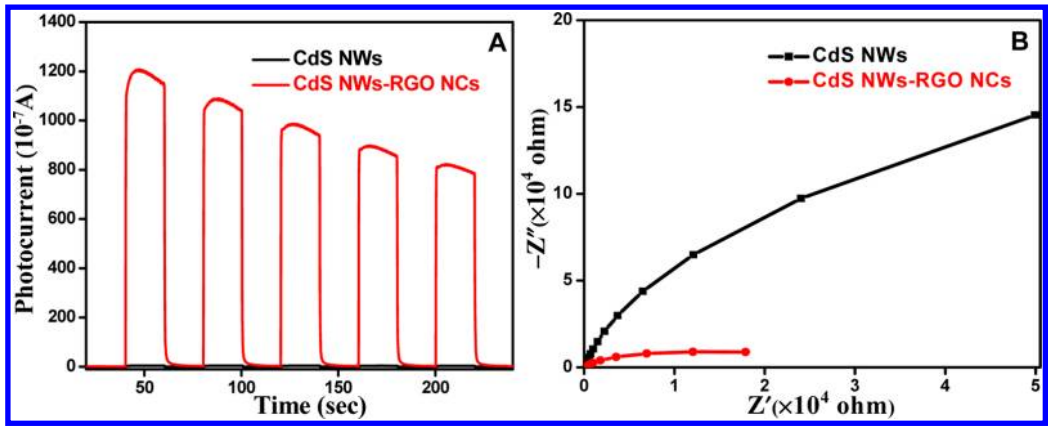

Figure 6. Transient photocurrent responses (A) and electrochemical impedance spectroscopy (EIS) Nyquist impedance plots (B) of CdS NWs and CdS NWs−RGO NCs in 0.2 M Na_2SO_4 (pH = 6.8) aqueous solution without bias versus Ag/AgCl under visible light irradiation (λ > 420 nm).

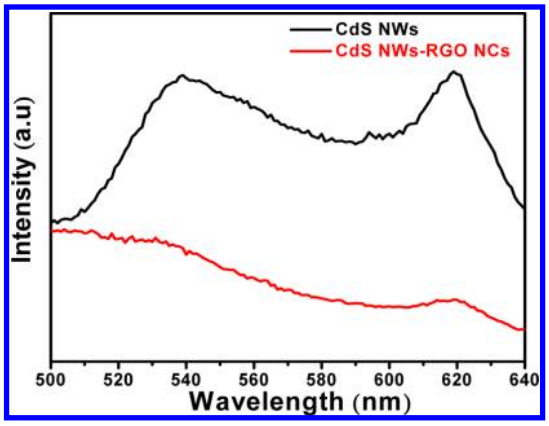

Figure 7. Photoluminescence (PL) spectra of CdS NWs and CdS NWs−RGO NCs with an excitation wavelength of 365 nm.

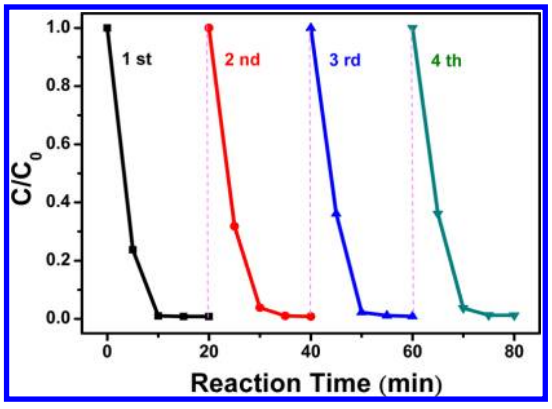

Figure 9. Cycling photocatalytic reduction of 4-nitroaniline over CdS NWs−RGO NCs under visible light irradiation (λ > 420 nm) with the addition of ammonium formate as a quencher for photogenerated holes and N_2 purge at room temperature in the aqueous phase.

reactions, which further verifies the photostability of the CdS NWs−RGO NCs.

The other factor contributing to the photoactivity enhancement for CdS NWs−RGO NCs is the increasing capability of adsorption by adding RGO into the matrix of CdS NWs. It is proven by UV−vis spectra of 4-NA after reaching the adsorption equilibrium in the dark over CdS NWs and CdS NWs−RGO NCs, as displayed in Figure S10 (in the Supporting Information). Such an enhanced adsorptivity of CdS NWs−RGO NCs over CdS NWs can be due to the higher specific surface area and pore volume of CdS NWs−RGO NCs than CdS NWs, which is evidenced in Table S1 (in the Supporting Information).

On the basis of the above discussion, the principle of photocatalytic selective reduction of nitro organics over the CdS NWs−RGO NCs photocatalyst can be delineated in Figure 10. Under the visible light irradiation (λ > 420 nm) with an inert N_2 purge, the electrons are excited from the valence band (VB) of CdS NWs in the framework of CdS NWs−RGO

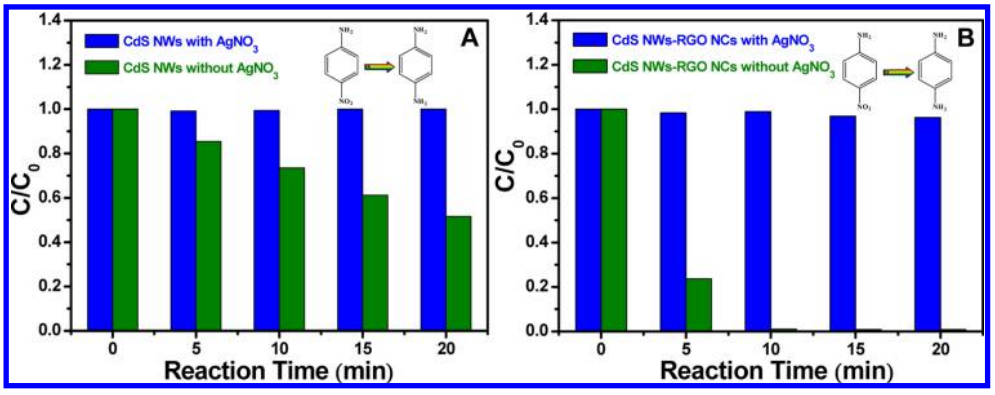

Figure 8. Controlled experiments using $AgNO_3$ as a scavenger for photogenerated electrons for 4-nitroaniline reduction over CdS NWs (A) and CdS NWs−RGO NCs (B) under visible light irradiation (λ > 420 nm) with the addition of ammonium formate as a quencher for photogenerated holes and N_2 purge at room temperature in the aqueous phase.

dx.doi.org/10.1021/jp400550t | J. Phys. Chem. C 2013, 117, 8251−8261

Figure 10. Schematic diagram illustrating the photocatalytic reduction process of nitro organics to amino organics under visible light irradiation ($\lambda > 420$ nm) with the addition of ammonium formate as a quencher for photogenerated holes and N_2 purge at room temperature in the aqueous phase.

NCs to the conduction band (CB) of CdS NWs, thereby forming the photogenerated electron−hole pairs. Simultaneously, the photogenerated positive holes, which generally contribute to oxidation reaction, are trapped by the quencher of ammonium formate. The reaction performed under N_2 purge along with using ammonium formate for quenching positive holes can guarantee the fact that the nitro organics would not undergo the oxidation reaction. On the other hand, due to the presence of RGO, the photogenerated electrons from CdS NWs can easily transfer to the RGO framework, by which the lifetime of photogenerated electrons is significantly improved. Meanwhile, the presence of RGO also increases the accumulating concentration of nitro organics over the surface of CdS NWs−RGO NCs. As a result, the adsorbed nitro organics can be effectively reduced to amino organics by accepting photogenerated electrons.

4. CONCLUDING REMARKS

To sum up, CdS NWs−RGO NCs are successfully synthesized via a simple and efficient electrostatic self-assembly method, followed by a hydrothermal reduction process. The photocatalytic performance of the as-prepared photocatalysts is examined by selective reduction of nitro organics to amino organics in the aqueous phase. The CdS NWs−RGO NCs exhibit significantly enhanced photoactivity as compared with the CdS nanowires (CdS NWs), which is because of the efficiently enhanced lifetime and transfer of photogenerated charge carriers due to the addition of RGO into the matrix of CdS NWs in a controlled manner. Furthermore, the presence of RGO also improves the adsorption capacity of CdS NWs−RGO NCs toward aromatic nitro organics. These two integrative factors synergistically result in the overall drastic photoactivity improvement of CdS NWs−RGO NCs toward selective reduction of nitro organics under visible light irradiation. It is hoped that our work could open a new doorway of synthesis of such 1-D semiconductor−2-D RGO composites as visible light photocatalysts for selective organic transformations, particularly for organic reduction reactions.

■ ASSOCIATED CONTENT

Supporting Information

Experimental details for synthesis of CdS nanowires (CdS NWs) and graphene oxide (GO), photograph of the experimental setup for photocatalytic activity testing, zeta potential analysis, zeta potential titration experiment spectra, Fourier transformed infrared spectroscopy (FT-IR) spectra, photographs of the CdS NWs and CdS NWs-RGO NCs, UV−vis absorption spectra of photocatalytic reduction of 4-nitroaniline, high-performance liquid chromatograph (HPLC) data, XRD patterns of the CdS NWs−RGO NCs before and after photoreduction, UV−vis absorption spectra of 4-nitroaniline over CdS NWs and CdS NWs−RGO NCs under adsorption equilibrium, column plots showing the remaining 4-nitroaniline in solution after being kept in the dark for 1 h until adsorption equilibrium of the 4-nitroaniline solution, and surface areas of CdS NWs and CdS NWs−RGO NCs. This material is available free of charge via the Internet at http://pubs.acs.org.

■ AUTHOR INFORMATION

Corresponding Author

*Tel./Fax: +86 591 83779326. E-mail: yjxu@fzu.edu.cn.

Notes

The authors declare no competing financial interest.

■ ACKNOWLEDGMENTS

The support by the National Natural Science Foundation of China (NSFC) (20903023, 20903022, 21173045), the Award Program for Minjiang Scholar Professorship, the Natural Science Foundation (NSF) of Fujian Province for Distinguished Young Investigator Grant (2012J06003), the Program for Changjiang Scholars and Innovative Research Team in Universities (PCSIRT0818), the Program for Returned High-Level Overseas Chinese Scholars of Fujian province, and the Project Sponsored by the Scientific Research Foundation for the Returned Overseas Chinese Scholars, State Education Ministry, is gratefully acknowledged.

■ REFERENCES

(1) Hoffmann, M. R.; Martin, S. T.; Choi, W.; Bahnemann, D. W. Environmental Applications of Semiconductor Photocatalysis. *Chem. Rev.* **1995**, *95*, 69−96.
(2) Kamat, P. V. Meeting the Clean Energy Demand: Nanostructure Architectures for Solar Energy Conversion. *J. Phys. Chem. C* **2007**, *111*, 2834−2860.
(3) Kamat, P. V. Photochemistry on Nonreactive and Reactive (Semiconductor) Surfaces. *Chem. Rev.* **1993**, *93*, 267−300.
(4) Chen, X.; Mao, S. S. Titanium Dioxide Nanomaterials: Synthesis, Properties, Modifications, and Applications. *Chem. Rev.* **2007**, *107*, 2891−2959.
(5) Fox, M. A.; Dulay, M. T. Heterogeneous Photocatalysis. *Chem. Rev.* **1993**, *93*, 341−357.
(6) Maldotti, A.; Molinari, A.; Amadelli, R. Photocatalysis with Organized Systems for the Oxofunctionalization of Hydrocarbons by O_2. *Chem. Rev.* **2002**, *102*, 3811−3836.
(7) Bard, A. J.; Fox, M. A. Artificial Photosynthesis: Solar Splitting of Water to Hydrogen and Oxygen. *Acc. Chem. Res.* **1995**, *28*, 141−145.
(8) Mills, A.; Davies, R. H.; Worsley, D. Water Purification by Semiconductor Photocatalysis. *Chem. Soc. Rev.* **1993**, *22*, 417−425.
(9) Chen, C.; Ma, W.; Zhao, J. Semiconductor-Mediated Photodegradation of Pollutants under Visible-Light Irradiation. *Chem. Soc. Rev.* **2010**, *39*, 4206−4219.

(10) Legrini, O.; Oliveros, E.; Braun, A. M. Photochemical Processes for Water Treatment. *Chem. Rev.* **1993**, *93*, 671−698.
(11) Zhang, N.; Liu, S.; Xu, Y.-J. Recent Progress on Metal Core@ Semiconductor Shell Nanocomposites as a Promising Type of Photocatalyst. *Nanoscale* **2012**, *4*, 2227−2238.
(12) Xu, Y.-J.; Zhuang, Y.; Fu, X. New Insight for Enhanced Photocatalytic Activity of TiO_2 by Doping Carbon Nanotubes: A Case Study on Degradation of Benzene and Methyl Orange. *J. Phys. Chem. C* **2010**, *114*, 2669−2676.
(13) Zhang, Y.; Tang, Z.-R.; Fu, X.; Xu, Y.-J. TiO_2−Graphene Nanocomposites for Gas-Phase Photocatalytic Degradation of Volatile Aromatic Pollutant: Is TiO_2−Graphene Truly Different from Other TiO_2−Carbon Composite Materials? *ACS Nano* **2010**, *4*, 7303−7314.
(14) Anpo, M. Utilization of TiO_2 Photocatalysts in Green Chemistry. *Pure Appl. Chem.* **2000**, *72*, 1265−1270.
(15) Zhang, N.; Zhang, Y.; Xu, Y. J. Recent Progress on Graphene-Based Photocatalysts: Current Status and Future Perspectives. *Nanoscale* **2012**, *4*, 5792−5813.
(16) Grätzel, M. Low Cost and Efficient Photovoltaic Conversion by Nanocrystalline Solar Cells. *Chem. Eng. Technol.* **1995**, *67*, 1300−1305.
(17) Gaya, U. I.; Abdullah, A. H. Heterogeneous Photocatalytic Degradation of Organic Contaminants over Titanium Dioxide: A Review of Fundamentals, Progress and Problems. *J. Photochem. Photobiol., C* **2008**, *9*, 1−12.
(18) Zhang, Y.; Tang, Z.-R.; Fu, X.; Xu, Y.-J. Nanocomposite of Ag−AgBr−TiO_2 as a Photoactive and Durable Catalyst for Degradation of Volatile Organic Compounds in the Gas Phase. *Appl. Catal., B* **2011**, *106*, 445−452.
(19) Fujishima, A.; Zhang, X.; Tryk, D. TiO_2 Photocatalysis and Related Surface Phenomena. *Surf. Sci. Rep.* **2008**, *63*, 515−582.
(20) Tada, H.; Kiyonaga, T.; Naya, S.-i. Rational Design and Applications of Highly Efficient Reaction Systems Photocatalyzed by Noble Metal Nanoparticle-Loaded Titanium(IV) Dioxide. *Chem. Soc. Rev.* **2009**, *38*, 1849−1858.
(21) Fox, M. A. Organic Heterogeneous Photocatalysis-Chemical Conversions Sensitized by Irradiated Semiconductors. *Acc. Chem. Res.* **1983**, *16*, 314−321.
(22) Zhang, Y.; Zhang, N.; Tang, Z.-R.; Xu, Y.-J. Transforming CdS into an Efficient Visible Light Photocatalyst for Selective Oxidation of Saturated Primary C−H Bonds under Ambient Conditions. *Chem. Sci.* **2012**, *3*, 2812−2822.
(23) Shiraishi, Y.; Hirai, T. Selective Organic Transformations on Titanium Oxide-Based Photocatalysts. *J. Photochem. Photobiol., C* **2008**, *9*, 157−170.
(24) Flores, S. O.; Rios-Bernij, O.; Valenzuela, M. A.; Cordova, I.; Gomez, R.; Gutierrez, R. Photocatalytic Reduction of Nitrobenzene over Titanium Dioxide: By-Product Identification and Possible Pathways. *Top. Catal.* **2007**, *44*, 507−511.
(25) Mahdavi, F.; Bruton, T. C.; Li, Y. Photoinduced Reduction of Nitro Compounds on Semiconductor Particles. *J. Org. Chem.* **1993**, *58*, 744−746.
(26) Ferry, J. L.; Glaze, W. H. Photocatalytic Reduction of Nitro Organics over Illuminated Titanium Dioxide: Role of the TiO_2 Surface. *Langmuir* **1998**, *14*, 3551−3555.
(27) Brezova, V.; Tarabek, P.; Dvoranova, D.; Stasko, A.; Biskupic, S. EPR Study of Photoinduced Reduction of Nitroso Compounds in Titanium Dioxide Suspensions. *J. Photochem. Photobiol., A* **2003**, *155*, 179−198.
(28) Tada, H.; Ishida, T.; Takao, A.; Ito, S. Drastic Enhancement of TiO_2-Photocatalyzed Reduction of Nitrobenzene by Loading Ag Clusters. *Langmuir* **2004**, *20*, 7898−7900.
(29) Maldotti, A.; Andreotti, L.; Molinari, A.; Tollari, S.; Penoni, A.; Cenini, S. Photochemical and Photocatalytic Reduction of Nitrobenzene in the Presence of Cyclohexene. *J. Photochem. Photobiol., A* **2000**, *133*, 129−133.
(30) Zhang, F. X.; Jin, R. C.; Chen, J. X.; Shao, C. Z.; Gao, W. L.; Li, L. D.; Guan, N. J. High Photocatalytic Activity and Selectivity for Nitrogen in Nitrate Reduction on Ag/TiO_2 Catalyst with Fine Silver Clusters. *J. Catal.* **2005**, *232*, 424−431.
(31) Xia, Y.; Yang, P.; Sun, Y.; Wu, Y.; Mayers, B.; Gates, B.; Yin, Y.; Kim, F.; Yan, H. One-Dimensional Nanostructures: Synthesis, Characterization, and Applications. *Adv. Mater.* **2003**, *15*, 353−389.
(32) Zhang, Y.; Tang, Z.-R.; Fu, X.; Xu, Y.-J. Engineering the Unique 2D Mat of Graphene to Achieve Graphene-TiO_2 Nanocomposite for Photocatalytic Selective Transformation: What Advantage does Graphene Have over Its Forebear Carbon Nanotube? *ACS Nano* **2011**, *5*, 7426−7435.
(33) Zhang, L.; Yu, J. C.; Mo, M.; Wu, L.; Kwong, K. W.; Li, Q. A General in Situ Hydrothermal Rolling-Up Formation of One-Dimensional, Single-Crystalline Lead Telluride Nanostructures. *Small* **2005**, *1*, 349−354.
(34) Yu, J. C.; Hu, X.; Li, Q.; Zhang, L. Microwave-Assisted Synthesis and In-Situ Self-Assembly of Coaxial Ag/C Nanocables. *Chem. Commun.* **2005**, 2704−2706.
(35) Xiao, F. An Efficient Layer-by-Layer Self-Assembly of Metal-TiO_2 Nanoring/Nanotube Heterostructures, M/T-NRNT (M = Au, Ag, Pt), for Versatile Catalytic Applications. *Chem. Commun.* **2012**, *48*, 6538−6540.
(36) Rao, C. N. R.; Govindaraj, A. Synthesis of Inorganic Nanotubes. *Adv. Mater.* **2009**, *21*, 4208−4233.
(37) Hochbaum, A. I.; Chen, R.; Delgado, R. D.; Liang, W.; Garnett, E. C.; Najarian, M.; Majumdar, A.; Yang, P. Enhanced Thermoelectric Performance of Rough Silicon Nanowires. *Nature* **2008**, *451*, 163−167.
(38) Huynh, W. U.; Dittmer, J. J.; Alivisatos, A. P. Hybrid Nanorod-Polymer Solar Cells. *Science* **2002**, *295*, 2425−2427.
(39) Wu, D.; Liu, J.; Zhao, X.; Li, A.; Chen, Y.; Ming, N. Sequence of Events for the Formation of Titanate Nanotubes, Nanofibers, Nanowires, and Nanobelts. *Chem. Mater.* **2005**, *18*, 547−553.
(40) Tian, B.; Zheng, X.; Kempa, T. J.; Fang, Y.; Yu, N.; Yu, G.; Huang, J.; Lieber, C. M. Coaxial Silicon Nanowires as Solar Cells and Nanoelectronic Power Sources. *Nature* **2007**, *449*, 885−889.
(41) Gautam, U. K.; Fang, X.; Bando, Y.; Zhan, J.; Golberg, D. Synthesis, Structure, and Multiply Enhanced Field-Emission Properties of Branched ZnS Nanotube−In Nanowire Core−Shell Heterostructures. *ACS Nano* **2008**, *2*, 1015−1021.
(42) McPhillips, J.; Murphy, A.; Jonsson, M. P.; Hendren, W. R.; Atkinson, R.; Höök, F.; Zayats, A. V.; Pollard, R. J. High-Performance Biosensing Using Arrays of Plasmonic Nanotubes. *ACS Nano* **2010**, *4*, 2210−2216.
(43) Wang, J.; Gudiksen, M. S.; Duan, X.; Cui, Y.; Lieber, C. M. Highly Polarized Photoluminescence and Photodetection from Single Indium Phosphide Nanowires. *Science* **2001**, *293*, 1455−1457.
(44) Wang, Z. L. Splendid One-Dimensional Nanostructures of Zinc Oxide: A New Nanomaterial Family for Nanotechnology. *ACS Nano* **2008**, *2*, 1987−1992.
(45) Wang, Y.; Jiang, X.; Xia, Y. A Solution-Phase, Precursor Route to Polycrystalline SnO_2 Nanowires that Can Be Used for Gas Sensing under Ambient Conditions. *J. Am. Chem. Soc.* **2003**, *125*, 16176−16177.
(46) Mor, G. K.; Varghese, O. K.; Paulose, M.; Shankar, K.; Grimes, C. A. A Review on Highly Ordered, Vertically Oriented TiO_2 Nanotube Arrays: Fabrication, Material Properties, and Solar Energy Applications. *Sol. Energy Mater. Sol. Cells* **2006**, *90*, 2011−2075.
(47) Tang, Z.-R.; Li, F.; Zhang, Y.; Fu, X.; Xu, Y.-J. Composites of Titanate Nanotube and Carbon Nanotube as Photocatalyst with High Mineralization Ratio for Gas-Phase Degradation of Volatile Aromatic Pollutant. *J. Phys. Chem. C* **2011**, *115*, 7880−7886.
(48) Tang, Z.-R.; Zhang, Y.; Xu, Y.-J. A Facile and High-Yield Approach to Synthesize One-Dimensional CeO_2 Nanotubes with Well-Shaped Hollow Interior as a Photocatalyst for Degradation of Toxic Pollutants. *RSC Adv.* **2011**, *1*, 1772−1777.
(49) Bavykin, D. V.; Walsh, F. C. Elongated Titanate Nanostructures and Their Applications. *Eur. J. Inorg. Chem.* **2009**, *2009*, 977−997.
(50) Tang, Z.-R.; Zhang, Y.; Xu, Y.-J. Tuning the Optical Property and Photocatalytic Performance of Titanate Nanotube toward Selective Oxidation of Alcohols under Ambient Conditions. *ACS Appl. Mater. Interfaces* **2012**, *4*, 1512−1520.

(51) Xiao, F. Layer-by-Layer Self-Assembly Construction of Highly Ordered Metal-TiO_2 Nanotube Arrays Heterostructures (M/TNTs, M = Au, Ag, Pt) with Tunable Catalytic Activities. *J. Phys. Chem. C* **2012**, *116*, 16487−16498.
(52) Liu, S.; Zhang, N.; Tang, Z.-R.; Xu, Y.-J. Synthesis of One-Dimensional CdS@TiO_2 Core−Shell Nanocomposites Photocatalyst for Selective Redox: The Dual Role of TiO_2 Shell. *ACS Appl. Mater. Interfaces* **2012**, *4*, 6378−6385.
(53) Shi, W.; Chopra, N. Controlled Fabrication of Photoactive Copper Oxide−Cobalt Oxide Nanowire Heterostructures for Efficient Phenol Photodegradation. *ACS Appl. Mater. Interfaces* **2012**, *4*, 5590−5607.
(54) Tongying, P.; Plashnitsa, V. V.; Petchsang, N.; Vietmeyer, F.; Ferraudi, G. J.; Krylova, G.; Kuno, M. Photocatalytic Hydrogen Generation Efficiencies in One-Dimensional CdSe Heterostructures. *J. Phys. Chem. Lett.* **2012**, *3*, 3234−3240.
(55) Schierhorn, M.; Boettcher, S. W.; Peet, J. H.; Matioli, E.; Bazan, G. C.; Stucky, G. D.; Moskovits, M. CdSe Nanorods Dominate Photocurrent of Hybrid CdSe−P3HT Photovoltaic Cell. *ACS Nano* **2010**, *4*, 6132−6136.
(56) Yong, C. K.; Noori, K.; Gao, Q.; Joyce, H. J.; Tan, H. H.; Jagadish, C.; Giustino, F.; Johnston, M. B.; Herz, L. M. Strong Carrier Lifetime Enhancement in GaAs Nanowires Coated with Semiconducting Polymer. *Nano Lett.* **2012**, *12*, 6293−6301.
(57) Lin, Y.-Y.; Chu, T.-H.; Li, S.-S.; Chuang, C.-H.; Chang, C.-H.; Su, W.-F.; Chang, C.-P.; Chu, M.-W.; Chen, C.-W. Interfacial Nanostructuring on the Performance of Polymer/TiO_2 Nanorod Bulk Heterojunction Solar Cells. *J. Am. Chem. Soc.* **2009**, *131*, 3644−3649.
(58) Ren, S.; Zhao, N.; Crawford, S. C.; Tambe, M.; Bulović, V.; Gradečak, S. Heterojunction Photovoltaics Using GaAs Nanowires and Conjugated Polymers. *Nano Lett.* **2010**, *11*, 408−413.
(59) Xiang, Q.; Yu, J.; Jaroniec, M. Graphene-Based Semiconductor Photocatalysts. *Chem. Soc. Rev.* **2012**, *41*, 782−796.
(60) Zhang, Y.; Zhang, N.; Tang, Z.-R.; Xu, Y.-J. Graphene Transforms Wide Band Gap ZnS to a Visible Light Photocatalyst. The New Role of Graphene as a Macromolecular Photosensitizer. *ACS Nano* **2012**, *6*, 9777−9789.
(61) Deng, S.; Tjoa, V.; Fan, H. M.; Tan, H. R.; Sayle, D. C.; Olivo, M.; Mhaisalkar, S.; Wei, J.; Sow, C. H. Reduced Graphene Oxide Conjugated Cu_2O Nanowire Mesocrystals for High-Performance NO_2 Gas Sensor. *J. Am. Chem. Soc.* **2012**, *134*, 4905−4917.
(62) Kumar, B.; Lee, K. Y.; Park, H.-K.; Chae, S. J.; Lee, Y. H.; Kim, S.-W. Controlled Growth of Semiconducting Nanowire, Nanowall, and Hybrid Nanostructures on Graphene for Piezoelectric Nanogenerators. *ACS Nano* **2011**, *5*, 4197−4204.
(63) Park, H.; Chang, S.; Jean, J.; Cheng, J. J.; Araujo, P. T.; Wang, M.; Bawendi, M. G.; Dresselhaus, M. S.; Bulović, V.; Kong, J.; Gradečak, S. Graphene Cathode-Based ZnO Nanowire Hybrid Solar Cells. *Nano Lett.* **2012**, *13*, 233−239.
(64) Jing, D.; Guo, L. A Novel Method for the Preparation of a Highly Stable and Active CdS Photocatalyst with a Special Surface Nanostructure. *J. Phys. Chem. B* **2006**, *110*, 11139−11145.
(65) Wang, L.-Y.; Wang, L.; Gao, F.; Yu, Z.-Y.; Wu, Z.-M. Application of Functionalized CdS Nanoparticles as Fluorescence Probe in the Determination of Nucleic Acids. *Analyst* **2002**, *127*, 977−980.
(66) Ma, R.-M.; Dai, L.; Qin, G.-G. High-Performance Nano-Schottky Diodes and Nano-MESFETs Made on Single CdS Nanobelts. *Nano Lett.* **2007**, *7*, 868−873.
(67) Wang, J.; Liu, G.; Merkoçi, A. Electrochemical Coding Technology for Simultaneous Detection of Multiple DNA Targets. *J. Am. Chem. Soc.* **2003**, *125*, 3214−3215.
(68) Zhang, N.; Zhang, Y.; Pan, X.; Fu, X.; Liu, S.; Xu, Y.-J. Assembly of CdS Nanoparticles on the Two-Dimensional Graphene Scaffold as Visible-Light-Driven Photocatalyst for Selective Organic Transformation under Ambient Conditions. *J. Phys. Chem. C* **2011**, *115*, 23501−23511.
(69) Wang, L.; Wei, H.; Fan, Y.; Gu, X.; Zhan, J. One-Dimensional CdS/α-Fe_2O_3 and CdS/Fe_3O_4 Heterostructures: Epitaxial and Non-epitaxial Growth and Photocatalytic Activity. *J. Phys. Chem. C* **2009**, *113*, 14119−14125.
(70) Hummers, W. S.; Offeman, R. E. Preparation of Graphitic Oxide. *J. Am. Chem. Soc.* **1958**, *80*, 1339−1339.
(71) Cote, L. J.; Kim, F.; Huang, J. Langmuir−Blodgett Assembly of Graphite Oxide Single Layers. *J. Am. Chem. Soc.* **2008**, *131*, 1043−1049.
(72) Kovtyukhova, N. I.; Ollivier, P. J.; Martin, B. R.; Mallouk, T. E.; Chizhik, S. A.; Buzaneva, E. V.; Gorchinskiy, A. D. Layer-by-Layer Assembly of Ultrathin Composite Films from Micron-Sized Graphite Oxide Sheets and Polycations. *Chem. Mater.* **1999**, *11*, 771−778.
(73) Pan, D.; Wang, S.; Zhao, B.; Wu, M.; Zhang, H.; Wang, Y.; Jiao, Z. Li Storage Properties of Disordered Graphene Nanosheets. *Chem. Mater.* **2009**, *21*, 3136−3142.
(74) Lee, J. S.; You, K. H.; Park, C. B. Highly Photoactive, Low Bandgap TiO_2 Nanoparticles Wrapped by Graphene. *Adv. Mater.* **2012**, *24*, 1084−1088.
(75) Li, D.; Muller, M. B.; Gilje, S.; Kaner, R. B.; Wallace, G. G. Processable Aqueous Dispersions of Graphene Nanosheets. *Nat. Nanotechnol.* **2008**, *3*, 101−105.
(76) Szabo, T.; Tombacz, E.; Illes, E.; Dekany, I. Enhanced Acidity and pH-Dependent Surface Charge Characterization of Successively Oxidized Graphite Oxides. *Carbon* **2006**, *44*, 537−545.
(77) Zhang, Y.; Zhang, N.; Tang, Z.-R.; Xu, Y.-J. Improving the Photocatalytic Performance of Graphene−TiO_2 Nanocomposites via a Combined Strategy of Decreasing Defects of Graphene and Increasing Interfacial Contact. *Phys. Chem. Chem. Phys.* **2012**, *14*, 9167−9175.
(78) Ren, Y.; Zhang, J.; Liu, Y.; Li, H.; Wei, H.; Li, B.; Wang, X. Synthesis and Superior Anode Performances of TiO_2−Carbon−RGO Composites in Lithium-Ion Batteries. *ACS Appl. Mater. Interfaces* **2012**, *4*, 4776−4780.
(79) Fan, W.; Lai, Q.; Zhang, Q.; Wang, Y. Nanocomposites of TiO_2 and Reduced Graphene Oxide as Efficient Photocatalysts for Hydrogen Evolution. *J. Phys. Chem. C* **2011**, *115*, 10694−10701.
(80) Peng, H.; Meng, L.; Niu, L.; Lu, Q. Simultaneous Reduction and Surface Functionalization of Graphene Oxide by Natural Cellulose with the Assistance of the Ionic Liquid. *J. Phys. Chem. C* **2012**, *116*, 16294−16299.
(81) Ng, Y. H.; Iwase, A.; Kudo, A.; Amal, R. Reducing Graphene Oxide on a Visible-Light $BiVO_4$ Photocatalyst for an Enhanced Photoelectrochemical Water Splitting. *J. Phys. Chem. Lett.* **2010**, *1*, 2607−2612.
(82) Woan, K.; Pyrgiotakis, G.; Sigmund, W. Photocatalytic Carbon-Nanotube−TiO_2 Composites. *Adv. Mater.* **2009**, *21*, 2233−2239.
(83) Zhang, N.; Zhang, Y.; Pan, X.; Yang, M.-Q.; Xu, Y.-J. Constructing Ternary CdS−Graphene−TiO_2 Hybrids on the Flatland of Graphene Oxide with Enhanced Visible-Light Photoactivity for Selective Transformation. *J. Phys. Chem. C* **2012**, *116*, 18023−18031.
(84) Xiao, F.-X. Construction of Highly Ordered ZnO−TiO_2 Nanotube Arrays (ZnO/TNTs) Heterostructure for Photocatalytic Application. *ACS Appl. Mater. Interfaces* **2012**, *4*, 7055−7063.
(85) Lightcap, I. V.; Kamat, P. V. Graphitic Design: Prospects of Graphene-Based Nanocomposites for Solar Energy Conversion, Storage, and Sensing. *Acc. Chem. Res.* **2012**. DOI: 10.1021/ar300248f.
(86) Liang, Y. T.; Vijayan, B. K.; Gray, K. A.; Hersam, M. C. Minimizing Graphene Defects Enhances Titania Nanocomposite-Based Photocatalytic Reduction of CO_2 for Improved Solar Fuel Production. *Nano Lett.* **2011**, *11*, 2865−2870.
(87) Liang, Y. T.; Vijayan, B. K.; Lyandres, O.; Gray, K. A.; Hersam, M. C. Effect of Dimensionality on the Photocatalytic Behavior of Carbon−Titania Nanosheet Composites: Charge Transfer at Nanomaterial Interfaces. *J. Phys. Chem. Lett.* **2012**, *3*, 1760−1765.
(88) Xu, D.; Liu, Z.; Liang, J.; Qian, Y. Solvothermal Synthesis of CdS Nanowires in a Mixed Solvent of Ethylenediamine and Dodecanethiol. *J. Phys. Chem. B* **2005**, *109*, 14344−14349.

(89) Xi, Y.; Zhou, J.; Guo, H.; Cai, C.; Lin, Z. Enhanced Photoluminescence in Core-Sheath CdS−PANI Coaxial Nanocables: A Charge Transfer Mechanism. *Chem. Phys. Lett.* **2005**, *412*, 60−64.
(90) Li, Y.; Liao, H.; Ding, Y.; Fan, Y.; Zhang, Y.; Qian, Y. Solvothermal Elemental Direct Reaction to CdE (E = S, Se, Te) Semiconductor Nanorod. *Inorg. Chem.* **1999**, *38*, 1382−1387.
(91) Shen, G.; Cho, J. H.; Yoo, J. K.; Yi, G.-C.; Lee, C. J. Synthesis of Single-Crystal CdS Microbelts Using a Modified Thermal Evaporation Method and Their Photoluminescence. *J. Phys. Chem. B* **2005**, *109*, 9294−9298.
(92) Kar, S.; Santra, S.; Heinrich, H. Fabrication of High Aspect Ratio Core−Shell CdS−Mn/ZnS Nanowires by a Two Step Solvothermal Process. *J. Phys. Chem. C* **2008**, *112*, 4036−4041.